Environmental Science & Technology

Article

pubs.acs.org/est

High Performance Monolithic Power Management System with Dynamic Maximum Power Point Tracking for Microbial Fuel Cells

Celal Erbay,[†] Salvador Carreon-Bautista,[†] Edgar Sanchez-Sinencio,[†] and Arum Han*[,†,‡]

[†]Department of Electrical and Computer Engineering, Texas A&M University, College Station, Texas 77843, United States
[‡]Department of Biomedical Engineering, Texas A&M University, College Station, Texas 77843, United States

ABSTRACT: Microbial fuel cell (MFC) that can directly generate electricity from organic waste or biomass is a promising renewable and clean technology. However, low power and low voltage output of MFCs typically do not allow directly operating most electrical applications, whether it is supplementing electricity to wastewater treatment plants or for powering autonomous wireless sensor networks. Power management systems (PMSs) can overcome this limitation by boosting the MFC output voltage and managing the power for maximum efficiency. We present a monolithic low-power-consuming PMS integrated circuit (IC) chip capable of dynamic maximum power point tracking (MPPT) to maximize the extracted power from MFCs, regardless of the power and voltage fluctuations from MFCs over time. The proposed PMS continuously detects the maximum power point (MPP) of the MFC and matches the load impedance of the PMS for maximum efficiency. The system also operates autonomously by directly drawing power from the MFC itself without any external power. The overall system efficiency, defined as the ratio between input energy from the MFC and output energy stored into the supercapacitor of the PMS, was 30%. As a demonstration, the PMS connected to a 240 mL two-chamber MFC (generating 0.4 V and 512 μW at MPP) successfully powered a wireless temperature sensor that requires a voltage of 2.5 V and consumes power of 85 mW each time it transmit the sensor data, and successfully transmitted a sensor reading every 7.5 min. The PMS also efficiently managed the power output of a lower-power producing MFC, demonstrating that the PMS works efficiently at various MFC power output level.

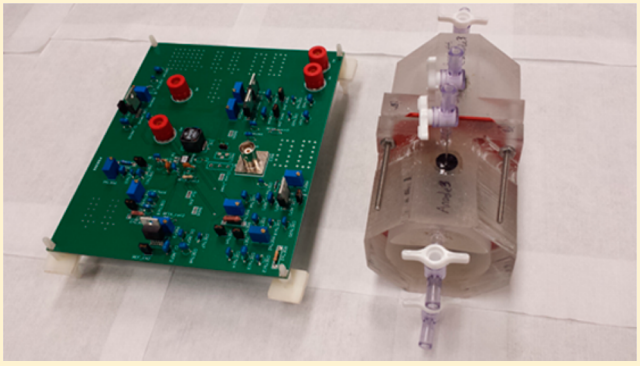

1. INTRODUCTION

Microbial fuel cells (MFCs) use electrochemically active bacteria (EAB) to convert organic substrates such as wastewater into electrical energy, and have been considered as a clean and promising renewable energy generation source.[1−3] However, their low power output per anode electrode surface area (100−2000 mW/m^2 at maximum power point (MPP)) and low voltage output (300−600 mV at MPP) make it difficult to directly power most electrical systems.[4] Fluctuating voltage and power level over time is another challenge for maximizing power extraction from MFCs. Large-scale MFCs can be built to overcome the low-power generation problem, however power output typically do not improve linearly due to scaling up issues,[5] and the low-voltage problem still persists. Connecting multiple MFCs in series has been demonstrated to increase the output voltage, however voltage reversal problems over time make such strategy inefficient beyond connecting about 2−3 MFCs in series, still limiting the voltage level that can be achieved.[6] Direct connection of capacitors in parallel or series to the MFC has been also tried, but this method does not allow dynamic matching of MFC internal resistance (R_{MFC}) and input impedance (Z_{in}) for maximum power extraction, and thus is inherently inefficient.[7]

The use of power management systems (PMS) are probably the most promising strategy in extracting maximum power from MFCs, as well as boosting the MFC output voltage level to a directly usable level.[8−17] PMSs are capable of increasing the MFC output voltage to an adequate level typically using DC-DC boost converter circuits[8−14] or charge pump circuits.[15−17] Such PMSs are commonly used in energy harvesting systems that generate low levels of power and voltage, such as for thermoelectric energy harvesting systems[18−20] and vibrational-energy harvesting systems.[21−23] For MFCs, charge pump circuits have been used as a voltage booster.[15−17] However, they require high MFC output voltage (~600 mV) to directly operate the charge pump efficiently due to its current limitation,[14] and the charging/discharging times are typically very long (more than 10 times) compared to boost converter.[16,17] DC-DC boost converters can overcome these limitations, and have been successfully integrated into PMSs managing MFC power.[8−14]

Received: March 24, 2014
Revised: September 28, 2014
Accepted: November 3, 2014
Published: November 3, 2014

dx.doi.org/10.1021/es501426j | Environ. Sci. Technol. 2014, 48, 13992−13999

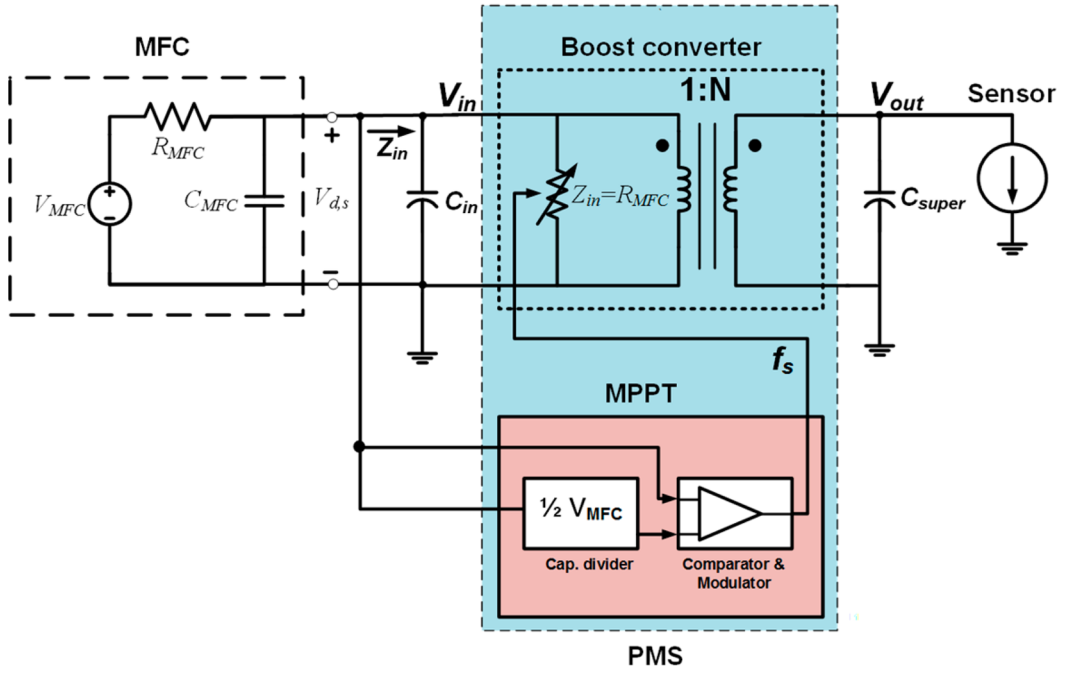

Figure 1. Proposed PMS for managing MFC power composed of a DC-DC boost converter block and a MPPT block.

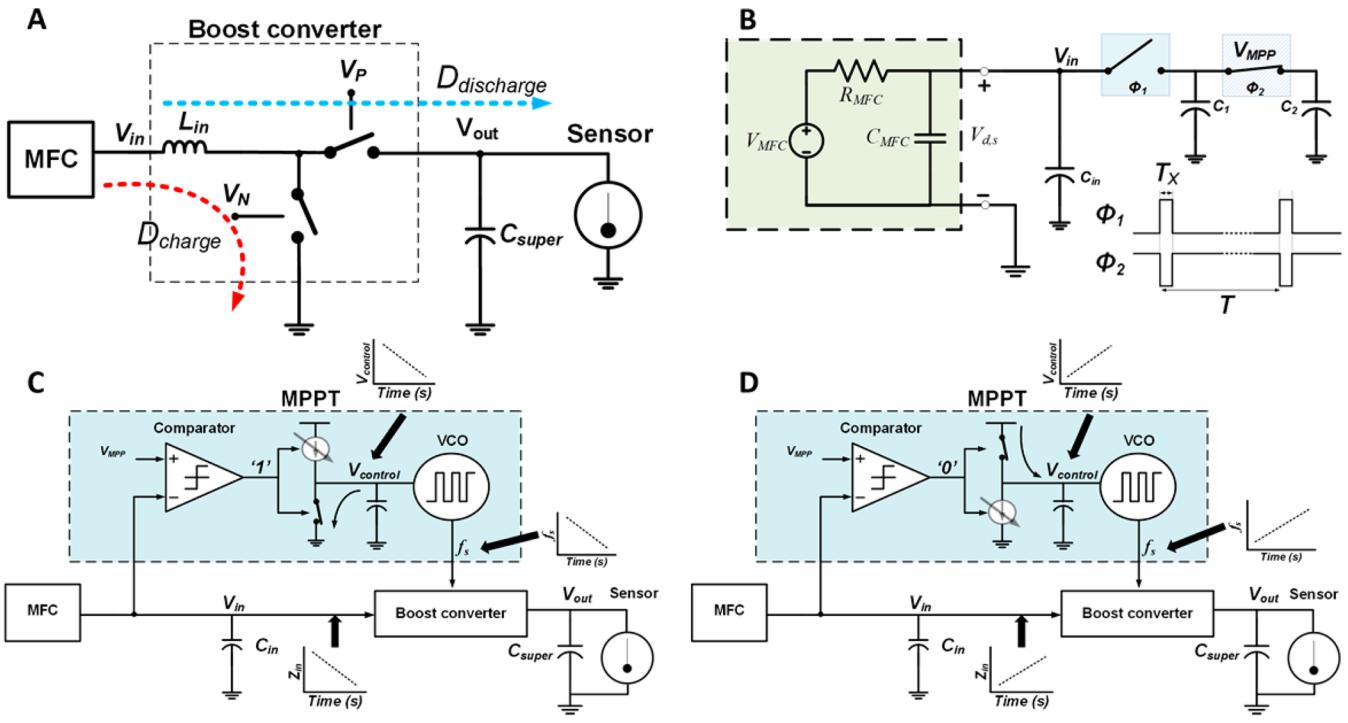

Figure 2. (A) Proposed synchronous DC−DC boost converter to step up the MFC input voltage to a higher output voltage (V_{out}). (B) Capacitive divider in the MPPT block to determine the V_{MPP}, which should be $^1/_2$ of V_{MFC}(V_{in}). (C) Dynamic MPPT scheme when Z_{in} is below R_{MFC}, which results in increasing the Z_{in}. (D) Dynamic MPPT scheme when Z_{in} is above R_{MFC}, which results in lowering the Z_{in}.

However, most PMSs used for MFC power management lack dynamic maximum power point tracking (MPPT) capabilities that allow continuously matching the load impedances of the PMSs to extract maximum power from MFCs, an important feature for MFCs as their power output typically changes over time. Woodward et al. showed that more than 50% of power may be lost across the internal resistance of an MFC if the load impedance is not matched.[24] An MFC can be viewed as a voltage source with internal resistance and capacitance (~160 μF). All three parameters (voltages, internal resistance, and internal capacitance) can change over time due to biofilm growth and fluctuations in operating conditions such as pH, temperature, and carbon substrate concentrations.[25,26] Thus, dynamically tracking the MPP is an essential scheme in PMSs for MFCs to maximize the power extraction efficiency. Wang et al. has presented an MPPT scheme for MFCs, however their system is composed of multiple external and discrete components that requires external power to operate

dx.doi.org/10.1021/es501426j | Environ. Sci. Technol. 2014, 48, 13992−13999

the PMS itself, resulting in low efficiency.[14] Yang et al. demonstrated an integrated circuit (IC) PMS, however due to the lack of MPPT feature, resulted in low system efficiency (4.29%) and long charging time (~2.3 h) of the supercapacitor used in the PMS.[12] A supercapacitor, also known as ultracapacitors or electric double layer capacitors, is an electrochemical capacitor and possesses a much higher capacitance value compared to conventional capacitors. Supercapacitors have much shorter charge/discharge cycles than rechargeable batteries, and can also tolerate more charge/discharge cycles.[27] These features make supercapacitors ideal for energy-harvesting systems, and thus will be used in our application to store energy harvested from MFCs through the PMS.

Here we present a highly efficient boost converter circuit with an MPPT scheme that can continuously detect the MPP of the MFC and match the load impedance of the PMS without using any external resistors by dynamically modulating the switching frequency of the boost converter and thus minimizing the time and power consumption for MPPT. The PMS circuit was fabricated in 0.5 μm CMOS technology, making this monolithic PMS IC chip system extremely power efficient so that the PMS could be operated using only the power from the MFC itself. Using this PMS and a supercapacitor, maximum energy was extracted at all times at an elevated voltage of 2.5 V, and was successfully used to periodically run a wireless temperature sensor.

2. MATERIALS AND METHODS

2.1. Power Management System (PMS). The PMS implemented here is an integrated synchronous DC-DC boost converter circuit in 0.5 μm CMOS technology, with dynamic MPPT capabilities (Figure 1). The boost converter block steps up the input voltage (V_{in}) from the MFC to a higher output voltage (V_{out}, set to 2.5 V here), where the output voltage (V_{out}) charges a 100 mF supercapacitor (C_{super}) until it has sufficient power to operate a wireless temperature sensor. The MPPT block continuously measures 1/2 of the MFC open circuit voltage (1/2 V_{MFC}) and uses this information to control the switching frequency of the boost converter to match the load impedance (Z_{in}) of the PMS to be equal to the internal resistance of the MFC (R_{MFC}), thus assuring maximum power transfer.

2.1.1. DC−DC Boost Converter Block. The synchronous DC−DC boost converter is a step-up DC−DC switching converter that increases the input voltage from the MFC (typically in the 300−600 mV range at MPP) to a desired voltage level (set to 2.5 V here) (Figure 2A). The boost converter operates by storing the MFC energy into an inductor (L_{in}) during the charging period (NMOS switch "on", PMOS switch "off"; D_{charge} = duty cycle of the charging period equal to t_{NMOS}/T_{period}). This stored energy is then discharged into the load supercapacitor (C_{super}) during the discharging period ($D_{discharge}$ = duty cycle of discharging period equal to t_{PMOS}/T_{period}). Both D_{charge} and $D_{discharge}$ are unitless, since they are the ratio of two time units. The PMS is designed to have a 50% duty cycle (D_{charge} = 0.5), hence $t_{NMOS} = 0.5 \times T_{period}$. The period duration is defined by the input impedance of the MFC ($R_{MFC} = Z_{in}$). Continuously repeating this cycle results in higher output voltage level. This voltage gain can be achieved as long as the output current requirements are minimal.

The voltage gain of the boost converter is approximated by eq 1:[18]

$$M \approx 1 + \frac{D_{charge}}{D_{discharge}} \quad (1)$$

where M is the conversion gain of the boost converter, D_{charge} and $D_{discharge}$ are the NMOS switch and PMOS switch duty cycles, respectively. Higher voltage gain can be achieved by minimizing the PMOS duty cycle compared to the NMOS duty cycle.

2.1.2. Maximum Power Point Tracking (MPPT) Block. The MFC is a voltage source that can be electrically modeled as having internal resistance (R_{MFC}), open circuit voltage (V_{MFC}), and capacitance (C_{MFC}). Since the delivered voltage from the MFC is DC, the internal capacitance is typically ignored in most PMS literature[13,14,28] as capacitors at DC behave as open circuit. Nonetheless, due to the method of locating the maximum power point through the open circuit voltage of the MFC in the presented PMS, knowing the internal capacitance is important for the presented MPPT scheme to be functioning properly. The equivalent circuit model of the MFC was used for the design of the PMS and the dynamic MPPT. The MPPT is implemented by first measuring the V_{MFC}, then calculating the voltage at maximum power point (V_{MPP} = 1/2 V_{MFC}), and then continuously comparing this V_{MPP} to V_{MFC}until the input impedance (Z_{in}) is matched to the internal resistance of the MFC (R_{MFC}).

When the switch ϕ_1 is "open" and switch ϕ_2 is "closed", the input capacitance (C_1) charges so that the input voltage V_{in} becomes equivalent to V_{MFC} (Figure 2B). When the switch ϕ_1 is closed and switch ϕ_2 is open, the charge in C_1 is divided by half and charges C_2, making V_{MPP} equal to 1/2 of V_{MFC}. Due to capacitor leakage from the equivalent series resistor (ESR), the aforementioned process for the attainment of V_{MPP} is performed continuously in order to maintain a correct value for MPPT. Due to the parallel capacitor (C_{MFC}) in the MFC electrical equivalent model, the MPP must take into account the RC time constant (τ_{MFC}) of the MFC source in order to correctly measure the MFC output voltage level (V_{MFC}). Thus, the switching period (T_X) associated with the first switch ϕ_1 has to be longer than the time constant of the τ_{MFC}. The value of T_x was tuned externally through a dedicated integrated one-shot circuit. Each sensing period (T_X) was set to ~1.8 s intervals and for a duration of approximately 200 ms. Measurement is performed through shorting the MFC between its terminals for a brief period of time (~2 s), then measuring the open circuit voltage and measuring the time the MFC requires to reset at nominal V_{MFC}.

The boost converter matches its input impedance to the MFC internal resistance R_{MFC} by varying the switching frequency of the switching transistor. The effect the switching frequency has on the input impedance (Z_{in}) is approximated by eq 2:[18]

$$Z_{in} \approx \frac{2 \cdot L_{in}}{D_{charge}^2 \cdot T_S} \quad (2)$$

where L_{in} is the inductor value, D_{charge} is the duty cycle for the NMOS transistor, and T_S is the period of the converter (detailed circuit diagram not shown here). The boost converter was designed with a fixed 50% duty cycle (D_{charge}) and an inductor value of 1.5 mH in order to minimize the switching frequency of the boost converter required for impedance matching. Detailed explanation of this part of the circuit design and calculations can be found in our previous work.[18] The

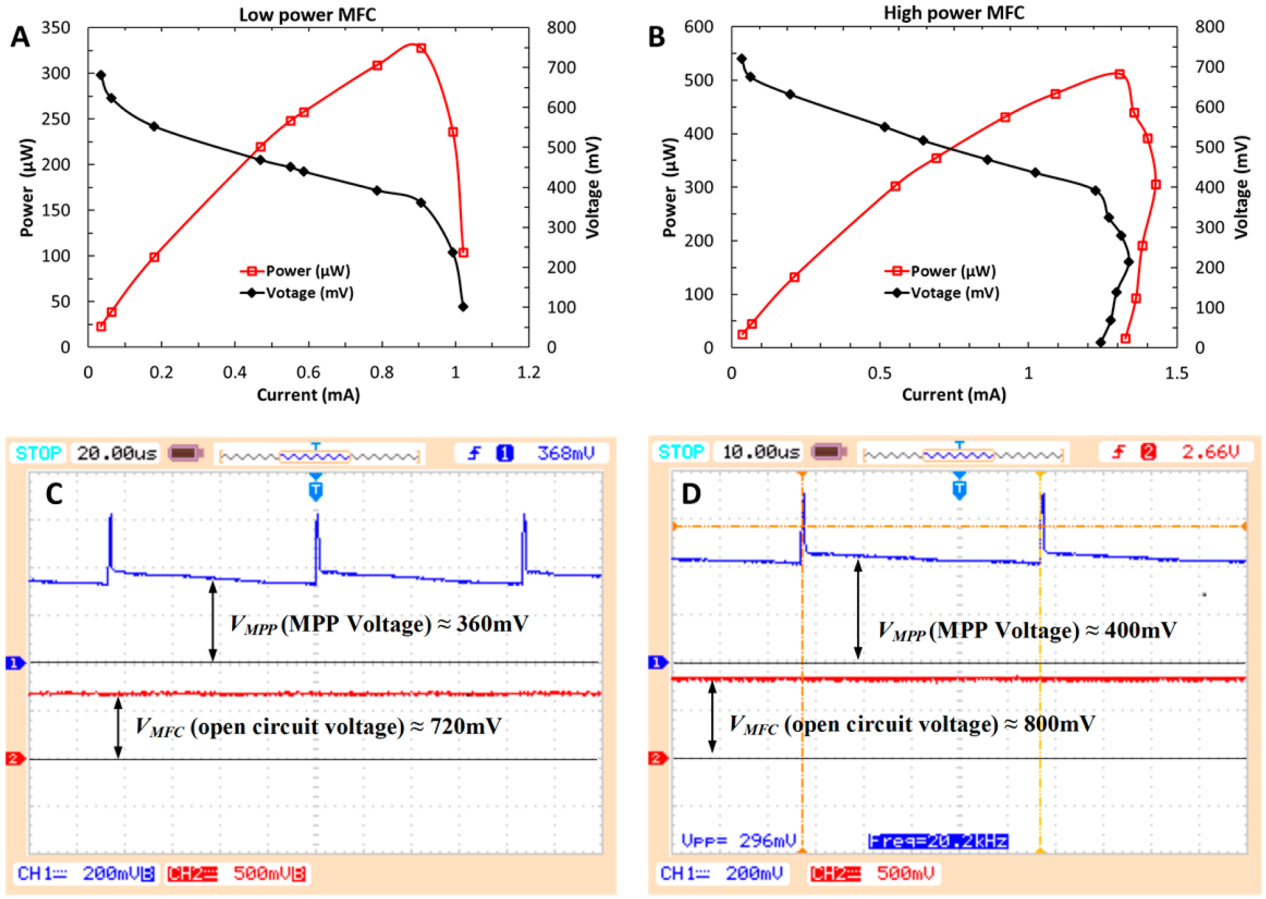

Figure 3. (A) Polarization curve obtained from the low-power MFC (LPMFC), showing power output of 328 μW and voltage output of 360 mV at MPP. (B) MPP voltage of 360 mV was successfully detected by the PMS when connected to the LPMFC having an open circuit voltage of 720 mV. (C) Polarization curve obtained from high-power MFC (HPMFC), showing power output of 512 μW and voltage output of 400 mV at MPP. D) MPP voltage (400 mV) was detected by the PMS when connected to the HPMFC having an open circuit voltage of 800 mV.

switching frequency to control the matching impedance is determined by the MPPT block.

Once the V_{MPP} has been identified, this voltage is compared to the V_{in} using a dynamic comparator, which then increases or decreases the control voltage (through a current steering charge pump) for a voltage controlled oscillator (VCO). This VCO then directly drives the boost converter's switching transistors to match the input impedance (see section 2.1.1). Figure 2C and 2D highlight the overall MPPT operating principle to achieve MPP. Figure 2C presents the condition when Z_{in} of the boost converter is higher than R_{MFC} and the loop dynamics of each functional components associated with this condition. In this case the $V_{control}$ decreases, resulting in lower voltage applied to the VCO, meaning the switching frequency (f_s) drops. This results in lower input impedance Z_{in}. The opposite condition is presented in Figure 2D, where Z_{in} of the boost converter is below R_{MFC}, in which case the $V_{control}$ increases, resulting in increased switching frequency (f_s). This results in higher input impedance Z_{in}. Power consumption for all components is minimum since most circuitry performs digitally.

2.2. PMS System Efficiency. The overall system efficiency of the PMS (η) was calculated based on the ratio of the output energy stored on the supercapacitor (E_{out}) and input energy generated by the MFC (E_{in}), as shown in the following eqs 3-6:

$$E_{out} = \frac{1}{2} \times C_{super} \times V_C^2 \quad (3)$$

$$E_{in} = P_{MFC} \times T_{MFC} \quad (4)$$

$$P_{MFC} = V_{MFC}^2/4R_{MFC} \quad (5)$$

$$\eta = \frac{E_{out}}{E_{in}} \times 100(\%) \quad (6)$$

where C_{super} is the capacitance of the supercapacitor (a 100 mF supercapacitor was used here), V_C is the voltage on the supercapacitor, P_{MFC} is the maximum power from the MFC, and T_{MFC} is the time duration. The voltage across the supercapacitor (V_C) and across the MFCs were recorded using an oscilloscope (DS1104B, Rigol Technologies Inc.).

The overall system efficiency strongly depends on the amount of power extracted from the MFC. The lower the MFC internal resistance and the lower the MFC internal capacitance, the more power will be available at the output of the MFC. Since the converter typically operates in steady state, the MFC capacitance does not come into consideration.

2.3. Using the PMS-Controlled MFC to Power a Wireless Temperature Sensor. The developed PMS controlling the MFC power/voltage output was tested to power a wireless temperature sensor (Monnit, Inc.) that uses a thermistor to accurately measure the temperature. The wireless temperature sensor required an operating voltage of 2−3.6 V (900 MHz operating frequency for wireless transmission) and power of 85 mW. The on-board lithium battery was removed

dx.doi.org/10.1021/es501426j | Environ. Sci. Technol. 2014, 48, 13992−13999

before testing so that the sensor was powered completely by the PMS-controlled MFC itself. The measured temperature is transmitted to a base station up to 250 feet away. The receiver base station was connected to a laptop computer.

2.4. MFC Construction and Operation. A two-chamber MFC was constructed from two 120 mL acrylic chambers separated with a PEM (Nafion 117, Ion Power Inc.). Carbon felt (Morgan, UK) was used as the anode (3 × 4 cm) and carbon cloth with Pt catalyst on one side (10 wt % Pt/C, 0.5 mg Pt/cm^2, ElectroChem, Inc.) was used as the cathode (3 × 4 cm). The anode chamber was inoculated with an anaerobic activated sludge (Austin Wastewater Plant). Autoclaved anaerobic nutrient mineral buffer (NMB, pH 7.0) solution[29] with acetate (1 g/L) was used as the carbon substrate containing media. To be able to test the developed PMS with MFCs showing different power output level, two MFC configurations were used. For the low-power output MFC (LPMFC) configuration, the cathode chamber was filled with phosphate buffer solution (PBS) (100 mM, pH 7.0) and continuously sparged with air. For the high-power output MFC (HPMFC) configuration, the catholyte was replaced with potassium ferricyanide (100 mM) to generate higher power. During the startup phase, the MFC was connected with an external resistor (1 kΩ) and the voltage across the resistor was monitored through a multiplexer (National Instruments) for continuous voltage measurements via a LabView (National Instruments) interface.[4,30,31] Polarization curve was obtained by varying the load resistances (100 Ω-10 kΩ).

3. RESULTS

3.1. PMS Correctly Determines Maximum Power Point (MPP) of the MFC. The polarization curve from the LPMFC after 6 months of operation showed a maximum power output of 328 μW at a current of 0.9 mA and a voltage of 360 mV (open circuit voltage of 720 mV) (Figure 3A). The maximum power from the HPMFC was 512 μW at a voltage of 400 mV (open circuit voltage of 800 mV) (Figure 3B). This is in line with a typical two-chamber MFC power performance when using wastewater inoculum and acetate as the carbon substrate.[32,33] These two MFCs were used to test how the developed PMS performs at two different MFC voltage and power levels.

The PMS circuit successfully identified the output voltage of the LPMFC at maximum power point as 360 mV (V_{MPP}), which was half of the LPMFC open circuit voltage (Figure 3C). This identified voltage was same as the MPP voltage obtained through a polarization curve that required varying the load resistors to find the MPP. The same successful result was accomplished when connecting the PMS to the HPMFC, which detected the correct V_{MPP} of 400 mV through the PMS circuit (Figure 3D). The screenshots show the MPPT capabilities of obtaining V_{MPP} when no load demand (PMS off) on the MFC is present. Once the PMS begins to extract power, the periods for T_X of 1.8 s and sampling periods of 200 ms are externally set through the one-shot circuit. The sensing period was made by setting a maximum ratio of disconnection to extraction period to no greater than 1/8. This limit would allow for minimum disruption on the power extraction from the PMS toward the MFC. Larger ratios would be possible but more considerations would have to be taken on sampling capacitor charge leakage and input buffer capacitor size. The developed MPPT function of the PMS continuously refreshes and corrects the optimum operating point for maximum power extraction, while minimizing power consumption. Thus, this dynamic MPPT scheme would be able to take into account any power variations of the MFC over time, resulting in maximum power efficiency.

3.2. Overall System Efficiency of the PMS. The overall system efficiency (η) is an important indicator to show the performance of the PMS and how much energy from the MFC is lost in the PMS circuit. The input energy (E_{in}) from the MFC and the output energy stored in the supercapacitor were measured over time until the voltage of the supercapacitor reached 2.5 V. When using the HPMFC (512 μW), the supercapacitor was charged to 2.5 V in 30 min and the average system efficiency was 30% over time (Figure 4A). System

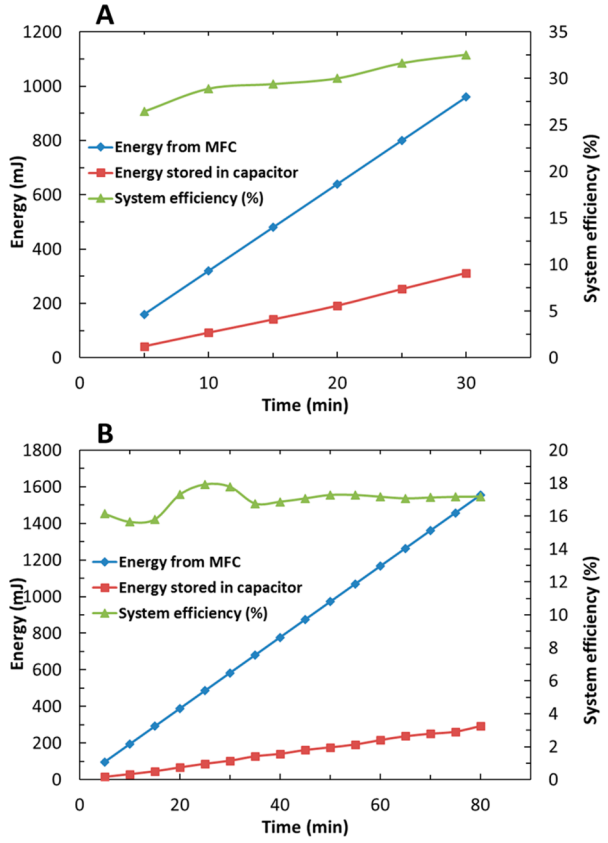

Figure 4. (A) The overall system efficiency of the PMS determined by the ratio of energy of the MFC and the energy stored in the supercapacitor (100 mF) when connected to a high-power MFC. Measurements were taken over the duration of the initial charging of the supercapacitor and periodic operating of the wireless temperature sensor. (B) System efficiency, energy from MFC, and energy stored in the supercapacitor during the initial charging stage of the supercapacitor when connected to a low-power MFC.

efficiency was slightly lower in the beginning due to the slow charging of the supercapacitor during the initial dynamic MPPT detection, however after detecting the MPP, increased over time and reached 33%. When using the LPMFC producing 328 μW, the system efficiency was 17% and the supercapacitor charging time to 2.5 V was initially 87.5 min (Figure 4B). In general, the PMS system efficiency has a direct correlation to the power output level, and thus higher system efficiencies were observed when the power output of the MFCs were higher.

3.3. Demonstration with Wireless Sensor Applications. Due to the low power production of most small-scale MFCs, it is quite difficult to run electronic devices directly and

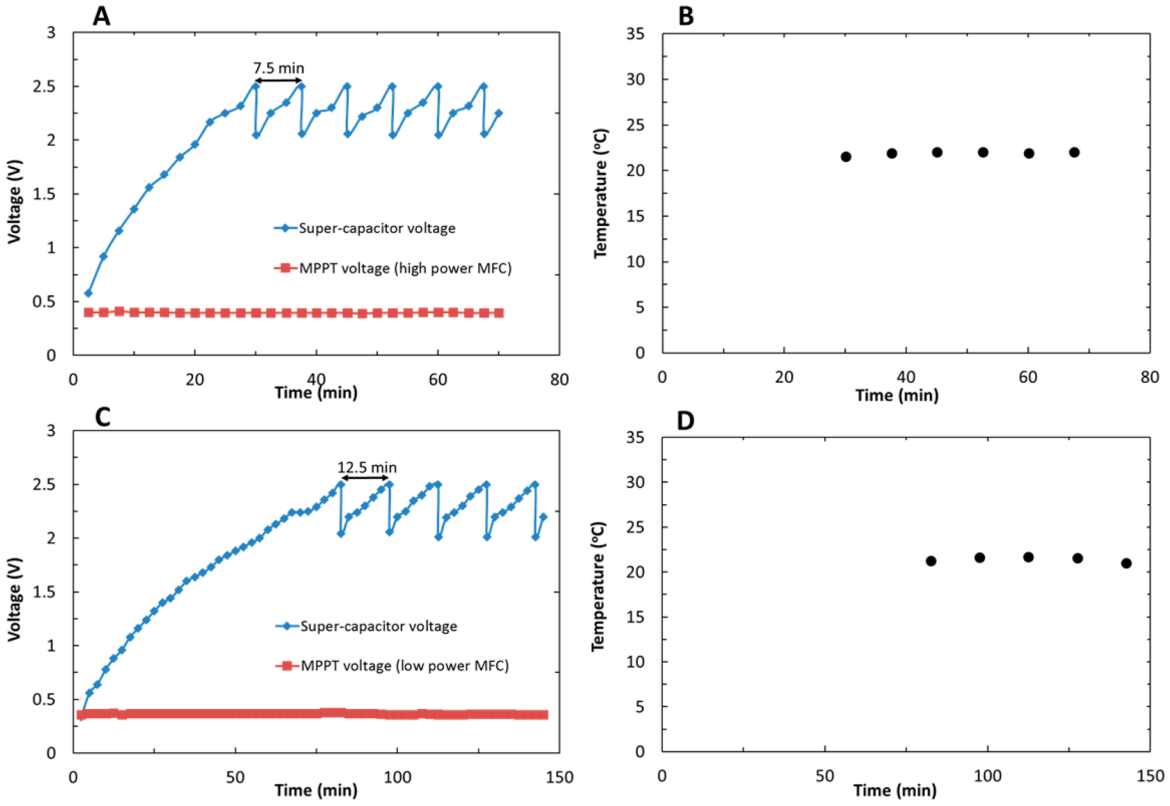

Figure 5. (A) The MPP voltage detected by the PMS and the supercapacitor voltage being charged to 2.5 V to directly power the wireless temperature sensor, when using the high-power MFC. (B) Wirelessly transmitted temperature data when using the high-power MFC. (C) Using the PMS with the low-power MFC. (D) Wireless temperature result when using the low-power MFC.

continuously. Wireless sensors or sensor nodes are ideal electronic applications that can be powered by MFCs, however even those low-power electronic devices require a PMS for voltage boosting and maximizing the utility of the power output. The wireless temperature sensor connected to the output of the PMS was successfully powered by the MFC periodically. The supercapacitor (100 mF) was first charged to 2.5 V, and then the wireless sensor was operated and the data transmitted to a base station connected to a laptop. Charging time of the supercapacitor to 2.5 V initially took 30 min and the MPPT voltage (400 mV) was linear all the time as shown in Figure 5A when using the HPMFC. Since the wireless sensor consumes around 85 mW, the supercapacitor voltage dropped to 2 V from 2.5 V each time a temperature reading was transmitted wirelessly. Then, it was recharged again to 2.5 V in 7.5 min to run the wireless temperature sensor again. Figure 5B shows the periodic wireless temperature reading from our laboratory.

When testing our PMS with the LPMFC that produces lower power, it can be seen that the power production is directly related to charging time, where it took a significantly longer 87.5 min to initially charge the supercapacitor to 2.5 V. The time interval between measurements was 12.5 min, almost 3 times longer compared to the case when using the HPMFC (Figure 5C). The periodic wireless temperature measurement result is shown in Figure 5D.

4. DISCUSSION

The high efficiency of the presented PMS is directly correlated with the dynamic MPPT scheme developed here. Alaraj et al. estimated the overall system efficiency to be 33.5% and 46.1% by using diode and transformer-based boost converters, respectively.[9] However, when calculating their system efficiency, the external power required to power their PMS was not considered. Donovan et al. showed a higher maximum efficiency (~60%) using the ratio of PMS output power and input power, but in the absence of the actual load used (wireless temperature sensor).[10] Similar measurement was also used in a dual cascaded DC-DC converter-based PMS, with efficiency was calculated to be 56.4% with fixed output loads, but again without considering the real load used for running their electronic applications.[11] Yang et al. utilized a commercially available DC-DC boost converter (LTC3108, Linear Technologies) and showed an overall system efficiency of 4.29% considering all losses due to PMS itself (thus being the most realistic case), however did not used any MPP.[12] We believe that the significantly higher overall system efficiency (7 times higher) achieved in the presented PMS (30%) under real load situation was due to the MPPT feature, integrated monolithic IC chip approach (versus commercially available discrete components), and the low-power CMOS chip design implemented in our PMS. Overall summary of efficiencies is summarized in Table 1. In a similar MFC application for wireless temperature sensor operation presented by Yang et al.,[12] it took initially 2.28 h to charge a supercapacitor (50 mF) to 3.3 V (wireless temperature sensor that consumes around 95 mW and operates at 3.3 V). During each sensor data transmission, the voltage dropped to 2.5 V, after which it took 1 h to reach back the 3.3 V. The main reason for this significantly longer charging time compared to our result can be explained by the lack of dynamically controlled MPPT, causing lower system efficiency (7 times lower than the PMS presented

Table 1. Comparison of Properties and Efficiencies of Different PMSs

input power from MFC (mW)	MPPT	output supercapacitor	overall system efficiency (%)	reference
~5.1	yes	1 F	46.1[a]	9
~2.4	no		60[b]	10
~3.4	no		56.4[b]	11
~0.8	no	50 mF	4.29	12
~0.5	yes	100 mF	30	this work

[a]External power was used, however not included in efficiency calculation. [b]Efficiency of PMS only, not overall system efficiency.

here). A significantly shorter charging/discharging cycle is advantageous in this kind of sensor applications.

Power consumption by the sensor is important in reducing the charge/discharge cycle time. Donowan et al. tested a wireless temperature sensor consuming only ~5 mW of power during data transmission (17 times lower power requirement) with a sediment MFC (SMFC).[10] The power production of the SMFC was 2.4 mW, which was 4.7 times higher than the MFC presented in this work. SMFC power production is normally larger than lab-scale two-chamber or one-chamber MFCs due to usage of significantly larger electrodes. Although using an MFC with significantly higher power output and using a low-power wireless temperature sensor compared to the ones used in this work, the interval of temperature measurement was ~20 min, longer than what the presented PMS-MFC achieved. Thus, the presented low-power PMS IC circuit with dynamic MPPT feature presents a promising solution toward highly efficient MFC power management, as well as be broadly used for managing power of other low-power energy harvesting systems such as from thermoelectric or piezoelectric-based energy harvesting systems.

Although the presented PMS enable maximum power extraction from MFCs, further improvement in the absolute MFC power output by improving and optimizing the numerous factors influencing MFC power output is still necessary for MFCs to be used in practice in the future.[34,35] While the proposed PMS here considers extracting power from a single MFC, the PMS has the potential to be used with stacks of MFCs. The MPPT in the developed PMS will only consider the equivalent resistor and equivalent capacitance from the arrayed MFC when calculating the maximum power extraction point, so array type implementations are possible with the presented PMS. A particular future work of interest is to implement a dynamically reconfigurable MFC stack, where the PMS constantly measures power production from each individual MFC units within the stack. With each sensing/measuring step, the stack can be reconfigured to deliver maximum power to the electronic load/storage unit. Another potential future works with the presented PMS is whether the MPPT scheme can be beneficial during the start-up phase of an MFC. The use of different load resistances has been shown to change the MFC start-up time,[36] thus the use of MPPT that matches the internal resistance of a MFC dynamically may reduce the start-up time for MFC to reach a steady-state voltage.

Such strategy might be able to be further expanded where the PMS and MPPT scheme can be used for creating an ideal electrochemical environment by optimizing the loading of the bacteria as directly as possible. The internal capacitance and resistance of an MFC are major contributors to the limited power output of MFCs. Future work on minimizing the internal capacitance through a dynamically controlled electronic system may be able to provide a more direct optimization of the power extraction from the bacteria, and thus further improve the overall system energy efficiency.

MFCs can produce only limited power and low voltages, typically not sufficient to directly power electronic systems. The monolithic PMS IC chip system presented here has the capability to boost the voltage output level to a directly usable level and continuously track the maximum power point through dynamic impedance matching circuitry to maximize the extracted power from the MFCs. The extracted power was stored into a supercapacitor and could periodically run electronic applications such as a wireless temperature sensor with short intervals. The PMS was operated by utilizing the power from the MFC without the need for any external power, and demonstrated an overall system efficiency of 30%. We expect that the developed low-power high-efficiency PMS system will be critical in managing power output of MFCs, as well as broadly utilized in other low-power low-voltage energy harvesting systems.

AUTHOR INFORMATION

Corresponding Author

*Phone: +1-979-845-9686; e-mail: arum.han@ece.tamu.edu.

Notes

The authors declare no competing financial interest.

ACKNOWLEDGMENTS

This work was supported by the Qatar National Research Foundation Grant No. NPRP 5-671-2-278 to A.H. The work was also partially supported by the Bill and Melinda Gates Foundation Grant No. OPP1044645 to A.H., and by Qualcomm and Silicon Labs support to E.S. The authors also thank MOSIS for the fabrication of the PMS. C.E. is supported by the Ministry of National Education of the Republic of Turkey.

REFERENCES

(1) Logan, B. E.; Hamelers, B.; Rozendal, R.; Schroder, U.; Keller, J.; Freguia, S.; Aelterman, P.; Verstraete, W.; Rabaey, K. Microbial fuel cells: Methodology and technology. *Environ. Sci. Technol.* **2006**, *40* (17), 5181−92.

(2) Lovley, D. R. The microbe electric: Conversion of organic matter to electricity. *Curr. Opin Biotechnol* **2008**, *19* (6), 564−71.

(3) He, Z.; Minteer, S. D.; Angenent, L. T. Electricity generation from artificial wastewater using an upflow microbial fuel cell. *Environ. Sci. Technol.* **2005**, *39* (14), 5262−5267.

(4) Hou, H.; Li, L.; de Figueiredo, P.; Han, A. Air-cathode microbial fuel cell array: A device for identifying and characterizing electrochemically active microbes. *Biosens. Bioelectron.* **2011**, *26* (5), 2680−4.

(5) Liu, H.; Cheng, S.; Huang, L.; Logan, B. E. Scale-up of membrane-free single-chamber microbial fuel cells. *J. Power Sources* **2008**, *179* (1), 274−279.

(6) Oh, S. E.; Logan, B. E. Voltage reversal during microbial fuel cell stack operation. *J. Power Sources* **2007**, *167* (1), 11−17.

(7) Kim, Y.; Hatzell, M. C.; Hutchinson, A. J.; Logan, B. E. Capturing power at higher voltages from arrays of microbial fuel cells without voltage reversal. *Environ. Sci. Technol.* **2011**, *4* (11), 4662−4667.

(8) Park, J.-D.; Ren, Z. Hysteresis controller based maximum power point tracking energy harvesting system for microbial fuel cells. *J. Power Sources* **2012**, *205* (0), 151−156.

(9) Alaraj, M.; Ren, Z. J.; Park, J.-D. Microbial fuel cell energy harvesting using synchronous flyback converter. *J. Power Sources* **2014**, *247* (0), 636−642.

(10) Donovan, C.; Dewan, A.; Heo, D.; Beyenal, H. Batteryless, wireless sensor powered by a sediment microbial fuel cell. *Environ. Sci. Technol.* **2008**, *42* (22), 8591−6.
(11) Donovan, C.; Dewan, A.; Peng, H.; Heo, D.; Beyenal, H. Power management system for a 2.5 W remote sensor powered by a sediment microbial fuel cell. *J. Power Sources* **2011**, *196* (3), 1171−1177.
(12) Yang, F.; Zhang, D.; Shimotori, T.; Wang, K.-C.; Huang, Y. Study of transformer-based power management system and its performance optimization for microbial fuel cells. *J. Power Sources* **2012**, *205* (0), 86−92.
(13) Park, J.-D.; Ren, Z. High efficiency energy harvesting from microbial fuel cells using a synchronous boost converter. *J. Power Sources* **2012**, *208* (0), 322−327.
(14) Wang, H.; Park, J.-D.; Ren, Z. Active energy harvesting from microbial fuel cells at the maximum power point without using resistors. *Environ. Sci. Technol.* **2012**, *46* (9), 5247−5252.
(15) Thomas, Y. R. J.; Picot, M.; Carer, A.; Berder, O.; Sentieys, O.; Barrière, F. A single sediment-microbial fuel cell powering a wireless telecommunication system. *J. Power Sources* **2013**, *241* (0), 703−708.
(16) Zhang, D.; Yang, F.; Shimotori, T.; Wang, K.-C.; Huang, Y. Performance evaluation of power management systems in microbial fuel cell-based energy harvesting applications for driving small electronic devices. *J. Power Sources* **2012**, *217* (0), 65−71.
(17) Meehan, A.; Hongwei, G.; Lewandowski, Z. Energy harvesting with microbial fuel cell and power management system. *IEEE Trans. Power Electron.* **2011**, *26* (1), 176−181.
(18) Carreon-Bautista, S.; Eladawy, A.; Mohieldin, A. N.; Sanchez-Sinencio, E. Boost converter with dynamic input impedance matching for energy harvesting with multi-array thermoelectric generators. *IEEE Trans. Ind. Electron.* **2014**, *61* (10), 5345−5353.
(19) Carlson, E. J.; Strunz, K.; Otis, B. P. A 20 mV input boost converter with efficient digital control for thermoelectric energy harvesting. *IEEE J. Solid-State Circuits* **2010**, *45* (4), 741−750.
(20) Jong-Pil, I.; Se-Won, W.; Seung-Tak, R.; Gyu-Hyeong, C. A 40 mV transformer-reuse self-startup boost converter with MPPT control for thermoelectric energy harvesting. *IEEE J. Solid-State Circuits* **2012**, *47* (12), 3055−3067.
(21) Elizabeth, K. R.; Fred, B.; Romy, F.; Paul, W. Powering a wireless sensor node with a vibration-driven piezoelectric energy harvester. *Smart Mater. Struct* **2011**, *20* (12), 125006.
(22) Ramadass, Y. K.; Chandrakasan, A. P. An efficient piezoelectric energy harvesting interface circuit using a bias-flip rectifier and shared inductor. *IEEE J. Solid-State Circuits* **2010**, *45* (1), 189−204.
(23) Yuan, R.; Arnold, D. P. An input-powered vibrational energy harvesting interface circuit with zero standby power. *IEEE Trans. Power Electron.* **2011**, *26* (12), 3524−3533.
(24) Woodward, L.; Perrier, M.; Srinivasan, B.; Pinto, R. P.; Tartakovsky, B. Comparison of real-time methods for maximizing power output in microbial fuel cells. *AIChE J.* **2010**, *56* (10), 2742−2750.
(25) Jadhav, G. S.; Ghangrekar, M. M. Performance of microbial fuel cell subjected to variation in pH, temperature, external load and substrate concentration. *Bioresour. Technol.* **2009**, *100* (2), 717−723.
(26) Borole, A. P.; Aaron, D.; Hamilton, C. Y.; Tsouris, C. Understanding long-term changes in microbial fuel cell performance using electrochemical impedance spectroscopy. *Energy Environ. Sci.* **2010**, *44* (7), 2740−2745.
(27) Winter, M.; Brodd, R. J. What are batteries, fuel cells, and supercapacitors? *Chem. Rev.* **2004**, *104* (10), 4245−4270.
(28) Jae-Do, P.; Zhiyong, R. Hysteresis-controller-based energy harvesting scheme for microbial fuel cells with parallel operation capability. *IEEE Trans. Energy Convers.* **2012**, *27* (3), 715−724.
(29) Chae, K. J.; Choi, M.; Ajayi, F. F.; Park, W.; Chang, I. S.; Kim, I. S. Mass transport through a proton exchange membrane (Nafion) in microbial fuel cells. *Energy Fuels* **2007**, *22* (1), 169−176.
(30) Hou, H.; Li, L.; Ceylan, C. U.; Haynes, A.; Cope, J.; Wilkinson, H. H.; Erbay, C.; Figueiredo, P. d.; Han, A. A microfluidic microbial fuel cell array that supports long-term multiplexed analyses of electricigens. *Lab Chip* **2012**, *12* (20), 4151−4159.
(31) Hou, H.; Li, L.; Cho, Y.; de Figueiredo, P.; Han, A. Microfabricated microbial fuel cell arrays reveal electrochemically active microbes. *PloS One* **2009**, *4* (8), e6570.
(32) Fan, Y.; Sharbrough, E.; Liu, H. Quantification of the internal resistance distribution of microbial fuel cells. *Environ. Sci. Technol.* **2008**, *42* (21), 8101−8107.
(33) Oh, S.-E.; Logan, B. Proton exchange membrane and electrode surface areas as factors that affect power generation in microbial fuel cells. *Appl. Microbiol. Biotechnol.* **2006**, *70* (2), 162−169.
(34) Aelterman, P.; Versichele, M.; Marzorati, M.; Boon, N.; Verstraete, W. Loading rate and external resistance control the electricity generation of microbial fuel cells with different three-dimensional anodes. *Bioresour. Technol.* **2008**, *99* (18), 8895−8902.
(35) Borole, A. P.; Reguera, G.; Ringeisen, B.; Wang, Z.-W.; Feng, Y.; Kim, B. H. Electroactive biofilms: Current status and future research needs. *Energy Environ. Sci.* **2011**, *4* (12), 4813−4834.
(36) Katuri, K. P.; Scott, K.; Head, I. M.; Picioreanu, C.; Curtis, T. P. Microbial fuel cells meet with external resistance. *Bioresour. Technol.* **2011**, *102* (3), 2758−2766.